

CycleSAM: One-Shot Surgical Scene Segmentation using Cycle-Consistent Feature Matching to Prompt SAM

Aditya Murali^{a,*}, Pietro Mascagni^{b,c}, Didier Mutter^b, Nicolas Padoy^{a,b}

^aUniversity of Strasbourg, CNRS, INSERM, ICube, UMR7357, Strasbourg, France

^bIHU Strasbourg, Strasbourg, France

^cFondazione Policlinico Universitario A. Gemelli IRCCS, Rome, Italy

The recently introduced Segment-Anything Model (SAM) has the potential to greatly accelerate the development of segmentation models. However, directly applying SAM to surgical images has key limitations including (1) the requirement of image-specific prompts at test-time, thereby preventing fully automated segmentation, and (2) ineffectiveness due to substantial domain gap between natural and surgical images. In this work, we propose **CycleSAM**, an approach for one-shot surgical scene segmentation that uses the training image-mask pair at test-time to automatically identify points in the test images that correspond to each object class, which can then be used to prompt SAM to produce object masks. To produce high-fidelity matches, we introduce a novel spatial cycle-consistency constraint that enforces point proposals in the test image to rematch to points within the object foreground region in the training image. Then, to address the domain gap, rather than directly using the visual features from SAM, we employ a ResNet50 encoder pretrained on surgical images in a self-supervised fashion, thereby maintaining high label-efficiency. We evaluate CycleSAM for one-shot segmentation on two diverse surgical semantic segmentation datasets, comprehensively outperforming baseline approaches and reaching up to 50% of fully-supervised performance.

1. Introduction

SAM [8] is a powerful general-purpose segmentation model that achieves excellent results in the natural image domain. Several works have successfully applied or adapted SAM for medical image segmentation [19, 11, 18, 3, 5] as well as surgical tool/scene segmentation [17, 13, 14, 21]. Yet, standard application of SAM requires user-provided prompts in the form of points, boxes, or masks at test-time, preventing fully-automated segmentation.

A few SAM-adaptation approaches have been proposed to bypass user prompts at test time [22, 23, 14]. [14] and [22] augment SAM with a custom prompt encoder, with the former using ground truth class names as prompts at test-time while the latter builds class prototype prompts by extracting foreground features for each object from the training images. However, these approaches are generally applied in a fully-supervised fashion and therefore still require a substantial amount segmentation annotations, which are extremely expensive in the surgical domain; moreover, they only achieve modest performance gains over traditional semantic segmentation models such as DeepLabv3+ and UNet.

In contrast, we are primarily interested in leveraging SAM for label-efficient segmentation. Our key insight, supported by [17, 13], is that despite the domain shift between natural and surgical images, SAM can still produce accurate masks if provided with good prompts. This decoupling of prompt and mask generation can enable SAM to achieve large gains over

traditional segmentation approaches in label-efficient settings, as even partial accuracy in prompt generation can translate to accurate masks. To this end, in this work we focus on the problem of **one-shot surgical scene segmentation**, addressing both complex anatomical structures and surgical tools in contrast to [22], which only considers the latter.

We build our approach, **CycleSAM**, as an extension of PerSAM [23], which uses feature matching to identify points in the test image that match each object class in the training image. To obtain higher-fidelity matches, we propose **CycleSelect**, a module for improved feature point matching consisting of (1) a spatial cycle-consistency masking function suppressing points that do not rematch to the object foreground region in the training image, (2) multiscale feature matching, and (3) a host of improvements to the point prompt sampling process including multiple foreground point selection and relevant negative point selection. Then, recognizing that feature-based point matching is highly dependent on a discriminative underlying feature space, we propose to augment the ViT feature extractor from SAM with MoCov2 [2] and DINO [1] self-supervised feature extractors pretrained on in-domain surgical images as in [15]. Finally, to tune the point features, we train linear feature projectors by enforcing an embedding-level contrastive loss between foreground and background point features.

We evaluate our approach on two challenging surgical scene segmentation datasets, Endoscapes-Seg50 [12] and CaDIS [4], selected specifically for their inclusion of anatomical structures as well as tools. In our experiments, we show that CycleSAM outperforms both traditional specialist and SAM-based segmentation approaches in the one-shot segmentation setting.

*Corresponding author: murali@unistra.fr

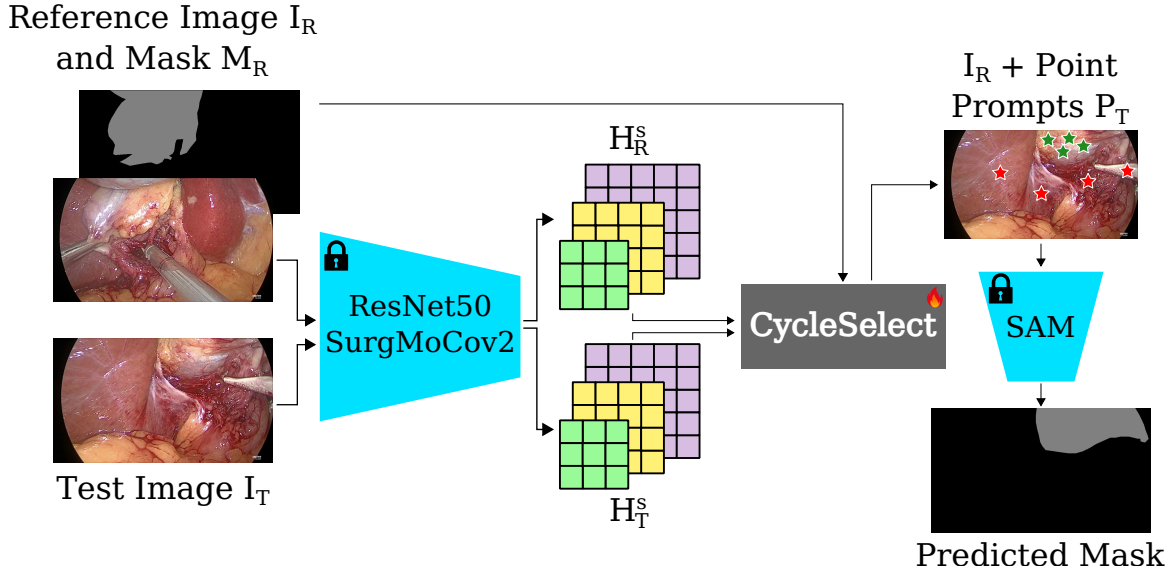


Fig. 1. An overview of CycleSAM. A ResNet50 encoder SSL-pretrained on surgical data is used to extract multi-scale features $\{\mathcal{H}_R^s \mid s \in [1..S]\}$, $\{\mathcal{H}_T^s \mid s \in [1..S]\}$ for the reference image I_R and test image I_T respectively. The multi-scale features are passed to the trainable CycleSelect module which generates both positive and negative point prompts for object c in the test image using cycle-consistent feature matching. Finally, these point prompts are passed to a frozen SAM model along with the original test image to produce a segmentation mask for the object.

Moreover, with just one labeled training image, CycleSAM reaches nearly 50% of fully-supervised performance, thus taking a large stride towards closing the performance gap.

In summary, our contributions are as follows:

1. We propose **CycleSAM**, a feature-matching based approach for 1-shot adaptation of SAM to complex surgical scene segmentation.
2. We introduce a novel feature matching module, **CycleSelect**, that uses spatial cycle consistency to greatly improve point correspondence across images.
3. We comprehensively outperform state-of-the-art SAM adaptation methods for label-efficient surgical scene segmentation.

2. Methods

In this section, we provide a detailed description of **CycleSAM**, which takes a reference (training) image I_R , corresponding reference mask \mathcal{M}_R , test image I_T , image encoder ϕ_{img} , and SAM model ϕ_{SAM} and outputs a binary mask \mathcal{M}_c for each object class $c \in [1..C]$. We first describe CycleSelect, a module that produces a set of point prompts \mathcal{P}_T^c in I_T for each object class c based on dense feature matching; each of the \mathcal{P}_T^c can then be passed to the SAM mask decoder ϕ_{SAM}^D . C different times to produce a mask for each class. Then, we describe the architecture and training process of CycleSAM consisting of (1) a feature similarity warm-up stage to refine the matching feature space and (2) the finetuning stage of PerSAM [23] that learns class-specific reweightings of the three masks $\hat{\mathcal{M}}_1^c$, $\hat{\mathcal{M}}_2^c$, and $\hat{\mathcal{M}}_3^c$ predicted by ϕ_{SAM}^D .

2.1. CycleSelect

CycleSelect, detailed in Algorithm 1, is based on the key assumption that points belonging to an object class c should

have similar feature representations across different images. It follows that given an image-mask pair as a reference, we can identify object points \mathcal{P}_T^c in a test image that match the reference foreground points \mathcal{P}_R^c by comparing their underlying feature representations.

The first step of CycleSelect is therefore to extract features for the reference image I_R and test image I_T with an image encoder ϕ_{img} , yielding feature maps \mathcal{H}_R and \mathcal{H}_T ; we then spatially resize these feature maps and the reference mask \mathcal{M}_R to $d_{\text{match}} \times d_{\text{match}}$. Next, to build a target feature h_{target}^c for each class c , we first evenly sample \tilde{X} points from the foreground region and use these points to index the reference feature map \mathcal{H}_R , yielding \tilde{X} point features h_{points}^c ; then, we average the features of all the foreground points, yielding a foreground summary feature h_{fg}^c , which we concatenate with h_{points}^c to yield $h_{\text{target}}^c \in \mathbb{R}^{X \times d_{\text{channel}}}$, where $X = \tilde{X} + 1$ and d_{channel} is the feature channel dimension.

Once we have computed h_{target}^c , we proceed to identify similar point features $h_i^c \in \mathcal{H}_T$. To do so, we compute a cosine similarity matrix $\mathcal{S}_{\text{all}} = h_{\text{target}}^c \cdot \mathcal{H}_T^T$ between the X target features and test feature map. Finally, we aggregate the similarities to each of the X target features into a global similarity map \mathcal{S} , where the indices of the highest values correspond to the points in the test image \mathcal{P}_T^c most likely to belong to the target class c .

Spatial Cycle-Consistency Masking. While we could directly use \mathcal{S} to sample point prompts, this often leads to spurious matches because the feature maps produced by ϕ_{img} are not sufficiently discriminative, particularly at the point granularity. To obtain a more robust similarity matrix, inspired by several prior works [6, 7, 9, 16], we introduce a spatial cycle consistency constraint that enforces matched points $p \in \mathcal{P}_T^c$ to rematch to points belonging within reference object. Intu-

Algorithm 1 CycleSelect Feature Similarity

Input: Image Encoder ϕ_{img} , Ref Img $\mathcal{I}_{\mathcal{R}}$, Test Img $\mathcal{I}_{\mathcal{T}}$, Ref Mask $\mathcal{M}_{\mathcal{R}}$, Obj Class c

$$\begin{aligned} \mathcal{H}_{\mathcal{R}} &\leftarrow \text{DOWNSAMPLE}(\phi_{\text{img}}(\mathcal{I}_{\mathcal{R}}), d_{\text{match}}); \quad \mathcal{H}_{\mathcal{T}} \leftarrow \text{DOWNSAMPLE}(\phi_{\text{img}}(\mathcal{I}_{\mathcal{T}}), d_{\text{match}}) \\ \mathcal{M}_{\mathcal{R}}^c &\leftarrow \text{DOWNSAMPLE}(\mathcal{M}_{\mathcal{R}}, d_{\text{match}}); \quad \mathcal{M}_{\mathcal{R}}^c[\mathcal{M}_{\mathcal{R}}^c \neq c] = 0; \quad \mathcal{M}_{\mathcal{R}}^c[\mathcal{M}_{\mathcal{R}}^c = c] = 1; \quad P_{\text{ref}}^c \leftarrow \text{ARGWHERE}(\mathcal{M}_{\mathcal{R}}^c) \\ P_{\text{sample}} &\leftarrow \text{POINTSAMPLE}(P_{\text{ref}}^c); \quad h_{\text{points}}^c \leftarrow \mathcal{H}_{\mathcal{R}}[P_{\text{sample}}] \\ h_{\text{fg}}^c &\leftarrow \text{MEAN}(\mathcal{H}_{\mathcal{R}}[\mathcal{M}_{\mathcal{R}}^c = 1]); \quad h_{\text{target}}^c \leftarrow \text{CONCAT}(h_{\text{points}}^c, h_{\text{fg}}^c); \quad \mathcal{S}_{\text{all}} \leftarrow h_{\text{target}}^c \cdot \mathcal{H}_{\mathcal{T}}^T \\ s &\leftarrow \text{ARGMAX}(\text{ABS}(\mathcal{S}), 0); \quad \lambda_{\text{agg}} \leftarrow \text{SIGN}(\mathcal{S}_{\text{all}}[s]) \\ \mathcal{S} &\leftarrow \lambda_{\text{agg}} \cdot \text{MAX}(\mathcal{S}_{\text{all}}, 0) + (1 - \lambda_{\text{agg}}) \cdot \text{MIN}(\mathcal{S}_{\text{all}}, 0) \\ \mathcal{S}_{\text{rematch}} &\leftarrow \text{FLATTEN}(\mathcal{H}_{\mathcal{T}}, 0, 2) \cdot \text{FLATTEN}(\mathcal{H}_{\mathcal{R}}, 0, 2)^T \\ \mathcal{M}_{\text{SCC}}^c &\leftarrow \mathbf{0}^{d_{\text{match}}^2}; \quad \mathcal{M}_{\text{SCC}}^c \leftarrow \mathcal{M}_{\mathcal{R}}[\text{ARGMAX}(\mathcal{S}_{\text{rematch}}, 1)] \\ \mathcal{M}_{\text{SCC}}^c &\leftarrow \text{RESHAPE}(\mathcal{M}_{\text{SCC}}^c, d_{\text{match}} \times d_{\text{match}}) \\ \mathcal{S}_{\text{SCC}}^c &\leftarrow \mathcal{S}; \quad \mathcal{S}_{\text{SCC}}^c[\mathcal{M}_{\text{SCC}}^c = 0] \leftarrow \mathcal{S}[\mathcal{M}_{\text{SCC}}^c = 0] - \lambda_{\text{SCC}} \end{aligned}$$

Algorithm 2 CycleSelect Multiscale Matching

$$\begin{aligned} \mathcal{H}_{\mathcal{R}} &\leftarrow \{\mathcal{H}_{\mathcal{R}}^s \in \mathbb{R}^{d_{\text{match}}^s \times d_{\text{match}}^s} \mid s \in [1..S]\}; \quad \mathcal{H}_{\mathcal{T}} \leftarrow \{\mathcal{H}_{\mathcal{T}}^s \in \\ &\mathbb{R}^{d_{\text{match}}^s \times d_{\text{match}}^s} \mid s \in [1..S]\} \\ \mathcal{S}_{\text{SCC}}^{\text{all}} &\leftarrow \{\text{RESIZE}(\text{CYCSELECT}(\mathcal{H}_{\mathcal{R}}^s, \mathcal{H}_{\mathcal{T}}^s, \text{RESIZE}(\mathcal{M}_{\mathcal{R}}^s, \\ &d_{\text{match}}^s))) \mid s \in [1..S], d_{\text{match}}^1\} \\ \mathcal{S}_{\text{SCC}} &\leftarrow \sum_{s \in [1..S]} W_{\text{scale}}^s * \mathcal{S}_{\text{SCC}}^s \end{aligned}$$

tively, such a constraint can help filter out poor matches that result from noisy feature maps and local ambiguities, and is particularly important for dealing with test images without the target object.

To integrate this cycle-consistency constraint into our approach, rather than simply removing points from $\mathcal{P}_{\mathcal{T}}^c$, we compute a cycle-consistency mask $\mathcal{M}_{\text{SCC}}^c$ in three steps: (1) we densely compute the cosine similarity $\mathcal{S}_{\text{rematch}} \in \mathbb{R}^{d_{\text{match}}^2 \times d_{\text{match}}^2}$ between all test and reference point features, (2) we find the index of the reference feature $h_{\mathcal{R}}^i$ that is most similar to each test feature $h_{\mathcal{T}}^j$, and (3) if the index of the rematched feature i is not in the reference mask $\mathcal{M}_{\mathcal{R}}$, we set the corresponding value in $\mathcal{M}_{\text{SCC}}^c$ to 1. We can then combine $\mathcal{M}_{\text{SCC}}^c$ and the original similarity matrix \mathcal{S}^c into a final cycle-consistent similarity matrix $\mathcal{S}_{\text{SCC}}^c$; to do so, we simply subtract a constant λ_{SCC} from the elements of \mathcal{S} masked by $\mathcal{M}_{\text{SCC}}^c$.

Multiscale Feature Matching To help deal with differing object sizes, we propose to incorporate multiscale modeling by repeating CycleSelect at different scales $s \in [1..S]$, yielding a set of similarity matrices $\{\mathcal{S}_{\text{SCC}}^s \mid s \in [1..S]\}$. We can then aggregate these similarities into a single similarity matrix \mathcal{S}_{SCC} after resizing each matrix to $d_{\text{match}} \times d_{\text{match}}$, as we do for the multiple target features. Algorithm 2 details the multiscale matching.

Point Prompt Sampling PerSAM [23] uses only a single point prompt per image; we instead select the top k foreground and background points from the final similarity matrix $\mathcal{S}_{\text{SCC}}^c$, resulting in a more informative prompt. Then, to boost

the utility of the background points, we cluster the similarity scores into 3 bins, and pick the top k points from the bin with the lowest scores. Intuitively, this clustering process separates the points into strong positive matches, ambiguous points, and strong negative matches. By picking the points with highest similarity from the strong negative matches, we can obtain informative exclusion point prompts while remaining confident that the selected points are indeed negatives. Finally, we threshold the positive matches with a per-class learnable threshold t_c ; we compute these thresholds during train-time as a weighted average of the similarity matrix $\mathcal{S}_{\text{SCC}}^c$ as follows:

$$\begin{aligned} t_c^+ &= \sum_{i,j} (\mathcal{S}_{\text{SCC}}^c)_{i,j} * (\mathcal{M}_{\mathcal{R}'}^c)_{i,j}; \quad t_c^- = \sum_{i,j} (\mathcal{S}_{\text{SCC}}^c)_{i,j} * (1 - \mathcal{M}_{\mathcal{R}'}^c)_{i,j} \\ t_c &= 0.5 * (t_c^+ + t_c^-) \end{aligned} \tag{1}$$

Following this process, we obtain $2k$ point prompts $\mathcal{P}_{\mathcal{T}}^c = \{\mathcal{P}_{\mathcal{T}}^{c,+}; \mathcal{P}_{\mathcal{T}}^{c,-}\}$ that we pass to the SAM mask decoder $\phi_{\text{SAM}}^{\mathcal{D}}$ to obtain masks M_1^c, M_2^c and M_3^c .

2.2. CycleSAM Architecture and Training

Figure 1 illustrates the overall architecture of CycleSAM, the main component of which is the trainable CycleSelect module. CycleSelect contains four different trainable components: (1) a Feature Projection block ϕ_{proj} comprising two linear feature projectors for each object class and feature scale (2CS in total), (2) a feature pyramid network (FPN) [10] ϕ_{FPN} to fuse multiscale image features, (3) per-class trainable scale weights $W_{\text{scale}} \in \mathbb{R}^{C \times S}$ to reweight the similarity matrices $\{\mathcal{S}_{\text{SCC}}^s \mid s \in [1..S]\}$ produced by the multiscale matching in CycleSelect, and (4) per-class trainable mask weights $W_{\text{mask}} \in \mathbb{R}^{C \times 3}$ as in [23] to reweight the three masks predicted by $\phi_{\text{SAM}}^{\mathcal{D}}$. To train CycleSAM in a one-shot fashion, we simply treat a copy of the reference image $\mathcal{I}_{\mathcal{R}}$ as the test image, referring to this copy as $\mathcal{I}_{\mathcal{R}'}$. We train in two stages: the first is a feature similarity warmup stage where we train ϕ_{proj} , ϕ_{FPN} and W_{scale} , and the second is the mask refinement training process of PerSAM [23] where we only train W_{mask} .

Feature Similarity Warmup PerSAM [23] directly uses feature maps $\mathcal{H}_{\mathcal{R}}$ and $\mathcal{H}_{\mathcal{T}}$ from ϕ_{img} , which in their case, is the

Table 1. Results on Endoscapes-Seg50 (ES50) and CaDIS. We split the baselines into 4 categories: (1) traditional segmentation approaches, for which we use DeepLabV3+ (DLV3P) as a representative baseline and experiment with various weight initializations and linear probing/finetuning, (2) SAM-based baseline approaches, including finetuning, adapter, and automatic prompt generation approaches, (3) our proposed CycleSAM and variants (backbone, initialization), and (4) a fully supervised DeepLabV3+ model to represent the ceiling performance. All performances from groups 1-3 are directly comparable.

Method	Finetune	ES50		CaDIS	
	Backbone	mIoU	mDice	mIoU	mDice
DLV3P-R50-SurgMoCov2	No	15.07	24.83	36.53	49.85
DLV3P-R50-SurgDINO	No	16.94	26.51	38.19	50.63
DLV3P-R50	Yes	14.65	22.62	43.20	54.76
DLV3P-R50-SurgMoCov2	Yes	15.70	24.05	41.61	54.39
DLV3P-R50-SurgDINO	Yes	14.05	21.79	43.30	55.93
SelfPromptSAM [20]	No	2.6	3.53	7.47	13.94
SurgicalSAM [22]	No	6.90	10.50	29.34	37.61
PerSAM [23]	No	4.42	7.97	25.01	34.56
PerSAM-F [23]	No	4.61	8.33	25.41	35.95
PerSAM-F-MedSAM [11, 23]	No	3.38	6.81	8.33	14.63
CycleSAM-ViT	No	8.17	14.26	31.82	42.89
CycleSAM-SurgDINO	No	15.52	22.13	35.91	47.85
CycleSAM-SurgMoCov2	No	16.40	24.05	33.76	44.49
CycleSAM-DLV3P-SurgDINO	No	20.56	28.48	47.37	61.78
CycleSAM-DLV3P-SurgMoCov2	No	22.34	30.86	44.21	59.40
DLV3P-R50-FullSup	Yes	45.02	57.60	83.18	90.61

ViT image encoder from ϕ_{SAM} , to construct a target feature h_{target} and compute a similarity matrix \mathcal{S} . However, when dealing with surgical images, the extracted feature space is far less discriminative due to substantial domain shift. As a result, we propose to instead use frozen SSL-pretrained ResNet50 encoders [15] for ϕ_{img} . Then, to improve the quality of the multiscale matching in CycleSelect, we further process the SSL features with a trainable FPN ϕ_{FPN} ; thus, the updated image encoder becomes $\phi_{\text{img}} = \phi_{\text{FPN}} \circ \phi_{\text{backbone}}$. Finally, because such SSL-pretrained encoders can lack the fine-grained precision of the SAM ViT encoder, which is specifically trained for pixel-level segmentation, we additionally apply asymmetric linear feature projectors to the test feature map $\mathcal{H}_{\mathcal{T}}$ and target feature h_{target} prior to computing \mathcal{S} : $W_{\text{feat_map}}, W_{\text{feat}} \in \mathbb{R}^{d_{\text{proj}} \times d_{\text{enc}}}$, where d_{enc} is the number of output channels of ϕ_{img} and d_{proj} is the final projected feature dimension. We include these projectors for each class c and feature scale s , yielding a total of $2CS$ projectors $\phi_{\text{proj}} : \{W_{\text{feat_map}}^{c,s}, W_{\text{feat}}^{c,s} \mid c \in [1..C], s \in [1..S]\}$.

To train these layers, we introduce a feature similarity contrastive loss \mathcal{L}_{sim} (see Algorithm 3) that maximizes the similarity of the target feature and foreground test features and minimizes that of the target feature and background features. Note that because we test image is simply the reference image during training, we also have a test mask $\mathcal{M}_{\mathcal{R}}$ that we use to separate foreground and background features. Finally, to train the multiscale weights W_{scale}^c , we simply treat the predicted similarity matrix $\mathcal{S}_{\text{SCC}}^c$ as a segmentation mask and compute an L1 loss against the ground truth mask $\mathcal{M}_{\mathcal{R}}^c$.

Algorithm 3 Feature Similarity Contrastive Loss

$$\begin{aligned}
 h_{\text{test}}^{c,\text{fg}} &\leftarrow \mathcal{H}_{\mathcal{R}'}[\mathcal{M}_{\mathcal{R}}^c = 1]; & h_{\text{test}}^{c,\text{bg}} &\leftarrow \mathcal{H}_{\mathcal{R}'}[\mathcal{M}_{\mathcal{R}}^c = 0] \\
 \mathcal{L}_{\text{sim}} &\leftarrow 0.5 * (1 - \cos(h_{\text{test}}^{c,\text{fg}}, h_{\text{target}}^c)) + 0.5 * \text{MAX}(\cos(h_{\text{test}}^{c,\text{bg}}, h_{\text{target}}^c))
 \end{aligned}$$

Mask Weighting After pre-training the feature similarity components ($\phi_{\text{FPN}}, \phi_{\text{proj}}, W_{\text{scale}}$), we freeze them and proceed to train W_{mask} . We follow the same process as [23], predicting a mask $\hat{\mathcal{M}}_{\mathcal{R}'}$ for $\mathcal{I}_{\mathcal{R}'}$ using CycleSAM and computing losses (Dice and Binary Cross-Entropy) against the ground-truth mask $\mathcal{M}_{\mathcal{R}'}$. We continue to asymmetrically augment $\mathcal{I}_{\mathcal{R}'}$ here to improve generalization.

3. Experiments and Results

We begin Section 3.1 by describing our evaluation datasets and metrics, then proceed to the main results. Then, in Section 3.2, we present an ablation study investigating the impact of CycleSAM’s improved prompt selection mechanisms.

3.1. Main Results

We evaluate all methods on two different surgical scene segmentation datasets, Endoscapes-Seg50 and CaDIS, and report mIoU^{NB} (excluding the background) and mean Dice score (mDice). Endoscapes-Seg50 [12] is a segmentation dataset for safe dissection in laparoscopic cholecystectomy that consists of 6 classes (5 anatomical structures and 1 tool class);

Table 2. Point Sampling Ablation Study on Endoscapes-Seg50.

Multiple Points ($k = 10$)	Negative Points	Learnable Threshold	mIoU
✗	✗	✗	13.68
✗	✓	✗	14.39
✓	✗	✗	16.58
✓	✓	✗	22.22
✗	✗	✓	14.24
✓	✓	✓	22.34

it presents a unique challenge due to the inclusion of fine-grained anatomical structures/windows (e.g. cystic plate, calot triangle). Meanwhile, CaDIS [4] is a dataset for scene segmentation in cataract surgery that, like Endoscapes-Seg50, also contains both anatomical structures and tools. CaDIS includes three different segmentation tasks of increasing granularity: in this work, since we already adopt the challenging 1-shot setup, we focus on the first task, an 8-class segmentation problem (4 anatomical structures, 1 tool class, 3 other). For training, we randomly select one image, ensuring that it contains all of the object classes, and using it for all of the methods.

Table 1 shows the results of all methods on both datasets, separated into four categories: (1) specialist models, for which we consider DeepLabV3Plus-ResNet50 (DLV3P-R50) as the base segmentation model and experiment with different backbone initializations (default, SurgMoCov2, and SurgDINO), (2) SAM-based approaches, including adaptation approaches [22, 11] and automatic prompt generation approaches [23, 20], (3) CycleSAM, also tested with various initializations for ϕ_{img} , and (4) a fully-supervised DeepLabV3Plus model to represent the ceiling performance. For SurgMoCov2 and SurgDINO, we use the weights provided by [15], and use Cholec80-pretrained models for the Endoscapes-Seg50 experiments and CaDIS-pretrained models for the CaDIS experiments. We also test CycleSAM variants using the original SAM ViT backbone as well as the 1-shot trained DLV3P-R50 models from group (1) to initialize ϕ_{img} .

Our best approach is CycleSAM initialized with the trained best-performing group 1 model, DLV3P-SurgMoCov2. CycleSAM-DLV3P-SurgMoCov2 not only outperforms all baseline methods but also achieves $\sim 50\%$ of fully supervised mIoU and $>50\%$ mDice on both datasets. Interestingly, we find that the best baseline methods are the group 1 specialist DeepLabV3Plus models, with the best models coming close to CycleSAM (difference of 5.40 mIoU for Endoscapes-Seg50, 4.07 mIoU for CaDIS). On the other hand, we comprehensively outperform existing SAM-based baseline methods, which are quite ineffective for one-shot surgical scene segmentation due to their reliance on the off-the-shelf feature representations. This is reiterated by studying CycleSAM-ViT, which directly uses the SAM ViT feature extractor as ϕ_{img} and performs similarly to the other SAM-based models. Furthermore, PerSAM-F-MedSAM, which uses MedSAM [11] as the underlying model rather than SAM, performs *worse* than the original PerSAM, highlighting the limitations of current off-the-shelf adaptations of SAM to medical domains. By flex-

ibly taking advantage of any domain-specific feature extractor, CycleSAM achieves massive performance gains over existing SAM-based approaches (+15.44 mIoU for Endoscapes-Seg50, +18.03 mIoU for CaDIS).

3.2. Prompt Selection Ablation Study

Table 2 shows the impact of our improved point sampling over the default approach of PerSAM [23]; by including 5 different points as prompts and including relevant negative points, we achieve an improvement of 8.54 mIoU on Endoscapes-Seg50, nearly doubling the performance.

4. Conclusion

We introduce CycleSAM, a method for one-shot adaptation of SAM for surgical scene segmentation using cycle-consistent feature matching. Our approach goes beyond the well-studied problem of tool segmentation and tackles two challenging surgical anatomy segmentation tasks. By leveraging surgical domain SSL-pretrained image encoders, CycleSAM effectively addresses the domain shift problem, vastly outperforming existing methods in the one-shot setting.

5. Acknowledgement

This work was supported by French state funds managed by the ANR within the National AI Chair program under Grant ANR-20-CHIA-0029-01 (Chair AI4ORSafety) and within the Investments for the future program under Grants ANR-10-IDEX-0002-02 (IdEx Unistra) and ANR-10-IAHU-02 (IHU Strasbourg). This work was granted access to the HPC resources of IDRIS under the allocation 2021-AD011011640R1 made by GENCI.

References

- [1] Caron, M., Touvron, H., Misra, I., Jégou, H., Mairal, J., Bojanowski, P., Joulin, A.: Emerging properties in self-supervised vision transformers. In: Proceedings of the IEEE/CVF international conference on computer vision. pp. 9650–9660 (2021)
- [2] Chen, X., Fan, H., Girshick, R., He, K.: Improved baselines with momentum contrastive learning. arXiv preprint arXiv:2003.04297 (2020)
- [3] Cheng, J., Ye, J., Deng, Z., Chen, J., Li, T., Wang, H., Su, Y., Huang, Z., Chen, J., Jiang, L., et al.: Sam-med2d. arXiv preprint arXiv:2308.16184 (2023)
- [4] Grammatikopoulou, M., Flouty, E., Kadkhodamohammadi, A., Quellec, G., Chow, A., Nehme, J., Luengo, I., Stoyanov, D.: Cadis: Cataract dataset for surgical rgb-image segmentation. Medical Image Analysis **71**, 102053 (2021)

- [5] Hu, X., Xu, X., Shi, Y.: How to efficiently adapt large segmentation model (sam) to medical images. arXiv preprint arXiv:2306.13731 (2023)
- [6] Hundt, A., Murali, A., Hubli, P., Liu, R., Gopalan, N., Gombolay, M., Hager, G.D.: ” good robot! now watch this! ”: Repurposing reinforcement learning for task-to-task transfer. In: 5th Annual Conference on Robot Learning (2021)
- [7] Jabri, A., Owens, A., Efros, A.A.: Space-time correspondence as a contrastive random walk. *Advances in Neural Information Processing Systems* (2020)
- [8] Kirillov, A., Mintun, E., Ravi, N., Mao, H., Rolland, C., Gustafson, L., Xiao, T., Whitehead, S., Berg, A.C., Lo, W.Y., et al.: Segment anything. arXiv preprint arXiv:2304.02643 (2023)
- [9] Lebailly, T., Stegmüller, T., Bozorgtabar, B., Thiran, J.P., Tuytelaars, T.: Cribo: Self-supervised learning via cross-image object-level bootstrapping. In: The Twelfth International Conference on Learning Representations (2023)
- [10] Lin, T.Y., Dollár, P., Girshick, R., He, K., Hariharan, B., Belongie, S.: Feature pyramid networks for object detection. In: *Proceedings of the IEEE conference on computer vision and pattern recognition*. pp. 2117–2125 (2017)
- [11] Ma, J., He, Y., Li, F., Han, L., You, C., Wang, B.: Segment anything in medical images. *Nature Communications* **15**(1), 654 (2024)
- [12] Murali, A., Alapatt, D., Mascagni, P., Vardazaryan, A., Garcia, A., Okamoto, N., Costamagna, G., Mutter, D., Marescaux, J., Dallemagne, B., et al.: The endoscopes dataset for surgical scene segmentation, object detection, and critical view of safety assessment: Official splits and benchmark. arXiv preprint arXiv:2312.12429 (2023)
- [13] Oguine, K.J., Soberanis-Mukul, R.D., Drenkow, N., Unberath, M.: From generalization to precision: Exploring sam for tool segmentation in surgical environments. arXiv preprint arXiv:2402.17972 (2024)
- [14] Paranjape, J.N., Nair, N.G., Sikder, S., Vedula, S.S., Patel, V.M.: Adap-tivesam: Towards efficient tuning of sam for surgical scene segmentation (2023)
- [15] Ramesh, S., Srivastav, V., Alapatt, D., Yu, T., Murali, A., Sestini, L., Nwoye, C.I., Hamoud, I., Sharma, S., Fleurentin, A., et al.: Dissecting self-supervised learning methods for surgical computer vision. *Medical Image Analysis* **88**, 102844 (2023)
- [16] Son, J.: Contrastive learning for space-time correspondence via self-cycle consistency. In: *Proceedings of the IEEE/CVF Conference on Computer Vision and Pattern Recognition (CVPR)*. pp. 14679–14688 (June 2022)
- [17] Wang, A., Islam, M., Xu, M., Zhang, Y., Ren, H.: Sam meets robotic surgery: An empirical study in robustness perspective. arXiv preprint arXiv:2304.14674 (2023)
- [18] Wang, C., Li, D., Wang, S., Zhang, C., Wang, Y., Liu, Y., Yang, G.: Sam-med: A medical image annotation framework based on large vision model. arXiv preprint arXiv:2307.05617 (2023)
- [19] Wu, J., Fu, R., Fang, H., Liu, Y., Wang, Z., Xu, Y., Jin, Y., Arbel, T.: Medical sam adapter: Adapting segment anything model for medical image segmentation. arXiv preprint arXiv:2304.12620 (2023)
- [20] Wu, Q., Zhang, Y., Elbatel, M.: Self-prompting large vision models for few-shot medical image segmentation. In: *MICCAI Workshop on Domain Adaptation and Representation Transfer*. pp. 156–167. Springer (2023)
- [21] Xie, W., Willems, N., Patil, S., Li, Y., Kumar, M.: Sam fewshot finetuning for anatomical segmentation in medical images. In: *Proceedings of the IEEE/CVF Winter Conference on Applications of Computer Vision (WACV)*. pp. 3253–3261 (January 2024)
- [22] Yue, W., Zhang, J., Hu, K., Xia, Y., Luo, J., Wang, Z.: Surgicalsam: Efficient class promptable surgical instrument segmentation (2024)
- [23] Zhang, R., Jiang, Z., Guo, Z., Yan, S., Pan, J., Dong, H., Gao, P., Li, H.: Personalize segment anything model with one shot. arXiv preprint arXiv:2305.03048 (2023)